International Journal of Science and Research (IJSR)
ISSN (Online): 2319-7064
Index Copernicus Value (2013): 6.14 | Impact Factor (2013): 4.438

Synthesis of Some Novel Surfactants Based On Di-Oleamide and Evaluation of Their Performance as Corrosion Inhibitors for X-70 Under sweet and Sour conditions

A. M. Al-Sabagh[2], M. A. Migahed[2], E. S. Gad[1]*, A. H. Halawa[1], H. M. Abd EL-Bary[1]

[1]Chemistry Department, Faculty of Science, Al-Azhar University, Cairo, Egypt
[2]Egyptian Petroleum Research Institute (EPRI), Nasr City, Cairo 11727, Egypt

*Corresponding Author: E. S. Gad (e_said56@yahoo. com)

Abstract: ***The main objective of this work was to examine the corrosion inhibition ability of three novel surfactant molecules synthesized fromN, N'- (azanediylbis (ethane-2, 1-diyl)) dioleamide which named (I, II and III). Their chemical structures were confirmed using FTIR and ^{1}HNMR spectroscopic methods. The surface active properties of the synthesized surfactants were calculated from surface tension measurements. Potentiodynamic polarization and electrochemical impedance spectroscopy (EIS) techniques were used to evaluate their performance as corrosion inhibitors for X-70 type tubing steel in deep oil wells formation water under sweet and sour environment at 25ºC. Polarization curves showed that by increasing theinhibitor concentration the corrosion current density was decreased, and the prepared surfactants acted as mixed type inhibitors. But the cathodic effect is more pronounced. Data obtained from EIS technique were analyzed to model the corrosion inhibition process through equivalent circuit (EC). Quantum chemical calculations based on ab initio method were performed on I, II and III. The molecular structural parameters, such as the frontier molecular orbital energy HOMO (highest occupied molecular orbital) and LUMO (lowest unoccupied molecular orbital), and the fraction of electrons (ΔN) transfer from inhibitor to carbon steel surface were calculated and discussed. Finally, the nature of the formed protective film was analyzed by SEM and EDX techniques. The results showed that the selected surfactants have good efficiencies as corrosion inhibitors for tubing steel in deep oil wells formation water under sweet and sour conditions.***

Keywords: Surfactants based on di-Oleamide, corrosion inhibitors, deep oil wells formation water, X-70 tubing steel, potentiodynamic polarization, EIS, SEM, EDX.

1. Introduction

Corrosion is a fundamental process playing an important role in economics and safety, particularly for metals **[1].** Carbon steel is widely used in many industrial applications especially petroleum industry from production to refinery and has remarkable economic and attractive materials for engineering applications owing to its low cost, easy availability and high mechanical strength. Many cases of extensive corrosion have occurred in production tubing, valves, and flow lines from the wellhead to the processing equipment. The cost of replacing, repairing and maintaining steel pipelines resulting from corrosion processing oil field is extremely expensive and time-consuming **[2, 3].** The development of corrosion inhibitors is based on organic compounds containing nitrogen, oxygen, sulphur atoms, and multiple bonds in the molecules that facilitate adsorption on the metal surface [**4,5].** Among them, the surfactant inhibitor has many advantages such as high inhibition efficiency, low price, low toxicity, easy productionand exhibit unique properties due to their amphiphilic molecule **[6–9].** The adsorption of the surfactant on the metal surface can markedly change the corrosion resisting property of the metal [**10, 11],** so the study of the relationship between the adsorption and corrosion inhibition is of great importance. These compounds are often simultaneously affected by both anodic and cathodic corrosion reactions; therefore, they are sometimes referred to as mixed-type corrosion inhibitors [**12–14].** The water content accompanying the oil production process has been found to be a significant factor in the internal corrosion of steel pipelines because the water contains many corrosive agents such as CO_2, H_2S, organic acids and salts [**15–21].** Both CO_2 and H_2S behave like weak acids. As such, they are able to provide oxidizing power and promote iron corrosion, establishing equilibrium between oxidation (Fe / Fe^{+2}) and reduction reactions. The most common reduction reaction in acid media is proton reduction ($2H^+ / H_2$). Carbon dioxide present in sweet wells forms a weak carbonic acid (H_2CO_3) solution in aqueous media which attack the steel pipeline and forms iron carbonate ($FeCO_3$) with the evolution of H_2 **[22].** The mechanism of H_2S contribution was proposed by Shoesmith et al **[23].** The corrosion reaction of iron with H_2S occurred mainly by a solid state reaction, via the reaction**:**

$$Fe + H_2S \longrightarrow FeS + H_2 \qquad (1)$$

To be effective, an inhibitor must displace water from the metal surface, interact with anodic or cathodic reaction sites to retard the oxidation and reduction corrosion reaction, prevent transportation of water and corrosion active species on the surface [**24].** In fact, introducing of

ethylene oxides into surfactant molecule (ethoxylation) increases the inhibitive effect of surfactant [**25].** The presence of these groups increases the solubility of surfactant and hence the extent of its adsorption on the metal surface increases and consequently its inhibitive action improves. The adsorption of the surfactant on the metal surface can markedly change the corrosion resisting property of the metal [**26,27],** so the study of the relationship between the adsorption and corrosion inhibition is of great importance. Quantum chemical calculations have been proved to be a very powerful tool for studying the inhibition mechanism [**28,29].** The present study is aimed to synthesis one nonionic and two cationic surfactants and evaluates their performance as corrosion inhibitors for carbon steel in oil wells formation water under sweet and sour environment. The choice of these compounds was based on molecular structure considerations that, these compounds contain hetero-atoms such as N and O, which induce greater adsorption of the inhibitor molecule onto the surface of carbon steel.

2. Experimental Method

2.1. Inhibitors

The three novel surfactants used in this study were synthesized in three steps as follow:

2.1.1. Synthesis of N,N'-(azanediylbis(ethane-2,1-diyl)) dioleamide.

0.04 mol of oleic acid in xylene (100 ml) was added to a solution of diethylenetriamine (2.06 g, 0.02 mol) in xylene (25 ml) drop wise by syringe under reflux. The reaction mixture was refluxed for 4h; the addition was complete after (1h). Then removing the solvent, the residue was recrystallized to give (A) as shown in **Scheme 1 [30].**

2.1.2. Ethoxylation.

The prepared N,N'-(azanediylbis(ethane-2,1-diyl)) dioleamide was charged in dry and closed vessel with continuous stirring while passing a stream of nitrogen gas through the system for 10 minutes to flush out air. The nitrogen stream was then replaced by ethylene oxide, 50 units of ethylene oxide was introduced to the namely (A) as shown in **Scheme 1** to produce non-ionic surfactant namely (I). The reaction took place in presence of triethylamine as a catalyst at 80–100 ^{0}C [**31, 32].**

2.1.3. Synthesis of Cationic Surfactants.

As shown in **Scheme 1**, quaternization reaction of compound (I) and different alkyl bromides (Isopropyl Bromide or 4-Bromo-Toluene) using an excess of alkyl bromide (25%) in acetone as solvent for 36 h at 80 ^{0}C to produce aliphatic cationic surfactants (II) and aromatic cationic surfactants (III) respectively. The mixture was allowed to cool-down. Then, the obtained mixture was further purified by diethyl ether and recrystallized **[33].**

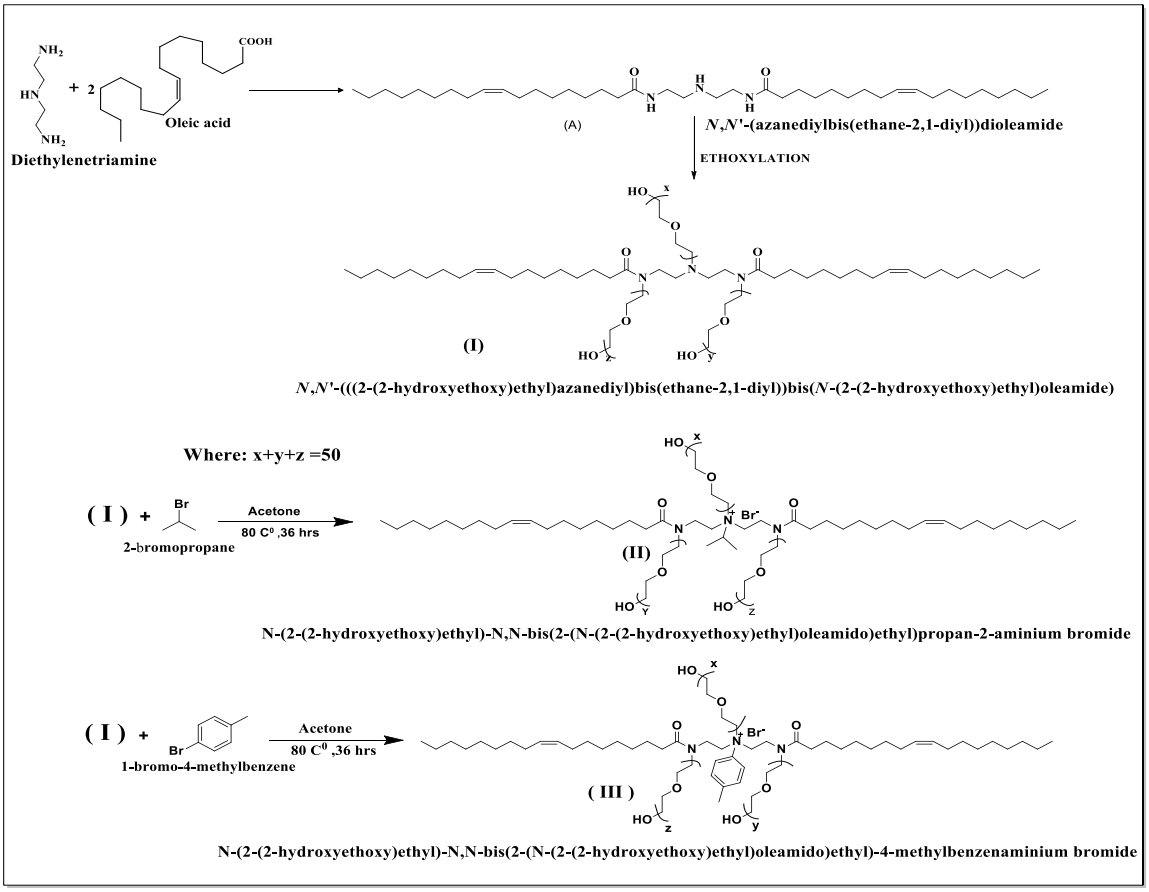

Scheme (1): Illustrate the formation of surfactants.

2.2. Steel Specimen

Tests were performed on a pipeline steel (X70) of the following chemical composition (wt. %) : 0. 07% C, 0. 3% Si, 1. 15% Mn, 0. 008% P, 0. 001%S, 0. 01% Ni, 0. 02% Cr, 0. 01% Mo, 0. 02% Cu, appropriate content of (V, Nb, Ti) and the remainder is Fe.

2.3. Solution Preparation

In the deep oil well formation waternaturally exists in the reservoir rocks before drilling, the following constituents [Na_2S (0. 006M), Na_2CO_3 (0. 05M) and HCl (1%)] were dissolved to prepare the test solution for the present work. The main components usually present in the most oil field water are inorganic compounds such as (sodium, calcium, magnesium, chloride, bicarbonate, and sulphate) and dissolved organic compounds. The chemical composition and physical properties of the used oil wells formation water are shown in **Table 1**.

2.4. Electrochemical Measurements

The electrochemical experiments were carried out in a conventional three-electrode cell with a platinum counter electrode (CE) and a saturated calomel electrode (SCE) as a reference electrode. The working electrode (WE) was a rod of API X70 steel pipeline embedded in glass holder using epoxy resin so that the flat surface was the only exposed surface in the electrode. The area of the working exposure surface was 0.79 cm^2. Before measurement, the electrode was abraded and rinsed with distilled water then immersed in a test solution at open circuit potential (OCP) for 3hours until a steady state was reached. All Electrochemical measurements were carried out using Voltalab 80 (Tacussel-radiometer PG Z402) controlled by Tacussel corrosion analysis software model (Volta master 4) at 25^0C.

2.4.1. Potentiodynamic Polarization Measurements

The potentiodynamic polarization measurements were obtained by changing the electrode potential automatically from -950 to -350 mV versus SCE with scan rate 2 mV s^{-1}.

2.4.2. Electrochemical Impedance Spectroscopy (EIS)

EIS measurements were performed in the frequency range between 100 kHz and 50 mHz using 10 steps per frequency decade at open circuit potential after 3hours of immersion time. AC signal with 20 mV amplitude peak to peak was used to perturb the system. EIS diagrams are given in Bode and Nyquist representations.

2.5. Surface Tension Measurement

The surface tension (γ) was measured using (Kruss K6 Tensiometer) type, a direct surface tension measurement using ring method) at 25 ^{0}C for various concentrations of the synthesized surfactants. All solutions were prepared in double distilled water with a surface tension equal 72 mN m^{-1} at 25 ^{0}C.

2. 6. Scanning Electron Microscopy

The surface examination was carried out using scanning electron microscope (JEOL JSM-5410, Japan). The energy of acceleration beam employed was 25 kV. All micrographs were taken at a magnification power (X 1000).

2.8. Energy Dispersive Analysis of X-rays (EDX)

EDX system attached with a JEOL JSM-5410 scanning electron microscope was used for elemental analysis or chemical characterization of the film formed on carbon steel surface before and after applying the synthesized inhibitor (III).

2.9. Quantum Chemical Study

The molecular structures of the inhibitors undertaken have been fully geometrically optimized via single point ab initiomethod (3-21G basis set) using Austin model 1 (AM1) with hyperchem quantum chemistry software [**34].**

3. Results and Discussion

3.1. Confirmation of Chemical Structure of the Prepared Inhibitors

3. 1. 1. FTIR Spectroscopy.

FTIR spectrum of N-(2-(2-hydroxyethoxy)ethyl)-N,N-bis(2-(N-(2-(2-hydroxyethoxy) ethyl)oleamido)ethyl)-4-methylbenzenaminium bromide as representative sample **Fig. 1** showed the following absorption bands:
1121 cm^{-1} (C–O band of the ethoxylated), 1377 cm^{-1} (C–N^+), 1657 cm^{-1} (C=O for amide group), 2854-2925 cm^{-1} (C–H aliphatic) and 3286 cm^{-1} (–OH group of ethoxylated primary amine). The FTIR spectrum confirmed the expected functional groups in the synthesized N-(2-(2-hydroxyethoxy)ethyl)–N,N-bis(2-(N-(2-(2-hydroxyethoxy) ethyl) oleamido) ethyl) -4-methylbenzenaminium bromide.

3.1.2. ^{1}H NMR Spectroscopy.

^{1}H NMR (DMSO-d_6) spectrum of N-(2-(2-hydroxyethoxy) ethyl)–N,N-bis(2-(N-(2-(2-hydroxyethoxy)ethyl)oleamido) ethyl) -4-methylbenzenaminium bromide as representative sample **Fig. 2** showed different bands:
CH_3- group at (a) 0.81 for terminal CH_3- of oleic acid, (b) 2.4 for CH_3- of tolyl group. The chemical shifts for CH_2-group at (a) 3.36 of the CH_2–group in the first ethylene oxide unit attached to 3° N, (b) 3.55 of the CH_2– group of repeated ethylene oxide units, (c) 1.2 of the CH_2 –group in the oleic acid, (d) 2.24 of the CH_2–group in adjacent to amide group and (e) 3.36 of the CH_2–group in the ethylene oxide unit attached to 4° N. The chemical shifts for CH-group at 5.28 ppm. Finally 7.063-7.78 (m, 4H, Ar-H). The data of ^{1}H NMR spectra confirmed the expected hydrogen proton distribution in the synthesized N-(2-(2-hydroxyethoxy)ethyl)–N,N-bis(2-(N-(2-(2-hydroxyethoxy) ethyl) oleamido) ethyl) -4-methylbenzenaminium bromide.

3.2. Polarization Measurements

Potentiodynamic polarization curves for API X70 steel pipeline in deep oil wells formation water under CO_2 and

H_2S environments containing various concentrations of inhibitor III as a representative sample at 25^0C are shown in **Fig. 3**. The corrosion current density values were estimated accurately by extrapolating both the cathodic and anodic linear region back to the corrosion potential. The degree of surface coverage (θ) and the inhibition efficiency (η_p %) were calculated using the following equations **[35]** :

$$\theta = [1 - (I / i_0)] \quad (2)$$

$$\eta_p \% = [1 - (i / i_0)] \times 100 \quad (3)$$

where i_0 and i are the corrosion current densities in the absence and presence of the inhibitor, respectively. The electrochemical corrosion parameters of corrosion current densities (I_{corr}), corrosion potential (E_{corr}), cathodic Tafel slope (b_c), anodic Tafel slope (b_a) and the inhibition efficiency (η_p%) as functions of inhibitors concentrations, are given in **Table 2**. These parameters could be explained as follows:

1. I_{corr} decreased with increasing the concentration of the three synthesized inhibitors which indicated that these compounds act as inhibitors, and the degree of inhibition depends on the concentrations of inhibitor.
2. The presence of the prepared surfactants are slightly shifted (E_{corr}) to negative and positive direction, which indicates that the synthesized compounds act as a mixed-type inhibitor **[35].**
3. b_c and b_a is slightly changed upon addition of inhibitors compared to blank, which implies that the inhibitors molecules are blocked for both cathodic and anodic sites resulting in an inhibition of the cathodic and anodic reactions.
4. η_p % of three synthesized inhibitors were calculated and listed in **Table 2**, which reveal that the inhibition efficiency increases with increasing of the inhibitor concentration up to 500 ppm. The order of inhibition efficiency decreased as follows: III > II > I.

3.3. Electrochemical Impedance Measurements

In order to gain more information about the corrosion inhibition phenomena, EIS measurements was carried out for API X70 steel pipeline in deep oil wells formation water under CO_2 and H_2S environments in the presence and absence of the synthesized surfactants. **Figs4, 5** show a typical set of Nyquist plots and Bode plots of the effect of the compound III as a representative sample in the absence and presence of various concentrations at 25 ^{0}C. Bode plots refer to the existence of an equivalent circuit. The increase of absolute impedance at low frequencies in Bode plot confirmed the higher protection with the increasing of inhibitor concentration, which is related to the adsorption of inhibitor on the carbon steel surface **[36].** Various parameters such as the charge transfer resistance (R_{ct}), double layer capacitance (C_{dl}) and percentage inhibition efficiency (η_I %) were calculated according to the following equations and listed in **Table 3 [37]** :

$$C_{dl} = [(1/2\pi f_{max.}) (1/R_{ct})] \quad (4)$$

$$\eta_I \% = [1- (R_{ct} / R_{ct} (inh)] \times 100 \quad (5)$$

where R_{ct} and R_{ct} (inh) are the charge transfer resistance values in the absence and presence of inhibitor, respectively. For analysis of the obtained impedance spectra, the equivalent circuit (EC) was obtained using EIS analyzer as shown in **Fig. 6** where (C_{dl}) is the double layer capacitance (R_s) is the solution resistance, (R_f) is the film resistance and (C_f) is the film capacitance. The obtained results conform the formation of a good protective film of the inhibitor molecules on carbon steel surface as indicated by following:

1. Increasing the value of charge transfer resistance (R_{ct}) with increasing the concentration of the synthesized surfactants indicating that the corrosion resistance of the X70 steel pipeline samples is mainly controlled by charge-transfer process.
2. Decreasing the value of double layer capacitance (C_{dl}) with increasing inhibitor concentration. This is due to the gradual replacement of water molecules in the double layer by the adsorbed inhibitor molecules, hence inhibiting the corrosion rate on carbon steel surface by adsorption mechanism [**38].**
3. It was found that the values of film resistance (R_f) were increased by increasing the inhibitor concentrations, while (C_f) values were decreased.
4. η_I % of three synthesized inhibitors increased with increasing inhibitor concentration up to 500 ppm. This is due to increasing the surface coverage by the inhibitor.
5. The corrosion inhibition efficiency of three synthesized inhibitors decreased in the following sequences: III > II > I.

3.4. Surface Active Properties Measurements

The CMC values of the synthesized surfactants were determined at 25 ^{0}C from the change in the slope of the plotted data of surface tension (γ) versus the natural logarithm of the solute molar concentration (-ln C) as shown in **Fig. 7**. The critical micelle concentration (CMC) is the point in concentration at which it becomes thermodynamically favorable for surfactant molecules in solution to form aggregates (micelles) in order to minimize interaction of either their head groups or their tail groups with the solvent. For the under investigation surfactants molecules in water, micellization is due to entropic considerations. Water molecules in close proximity to the hydrophobic group of the surfactant molecules take on a certain ordered configuration, which is entropically unfavorable. Once the surfactant concentration reaches a certain level (CMC), the hydrophobic tail groups forming surfactant micelles. Surface tension plots indicate that each surfactant is molecularly dispersed at low concentration, leading to a reduction in surface tension until certain concentration is reached the surfactant molecules form micelles, which are in equilibrium with the free surfactant molecules. The CMC values were determined from **Fig. 7** and listed in **Table 4**. It is obvious that the increase in hydrophobic chain length (present in the three prepared surfactants) decreases the values of the CMC [**39].** The organic character of the hydrophobic chains in the surfactant molecules increases the repulsion between these molecules and the aqueous phase. Also, hydrophobic

moieties on the head group (Isopropyl and Toluene) in surfactant (II and III) respectively increase the repulsion between the surfactant molecules and the aqueous phase. Hence, the increase in repulsion between the surfactant molecules and the aqueous phase increases the tendency of the surfactant molecules toward adsorption at the air–water interface. That causes fast saturation of the interface by the adsorbed molecules. As a result, it is expected that increasing the hydrophobic chain length will increase the adsorption of the molecules at the interface and will also increase the tendency of the molecules toward micellization in the bulk of their solutions **[40].** The maximum surface excess concentration (Γ_{max}) in mol/cm^2 was calculated from the following relationship [**41]:**

$$\Gamma_{max} = -(1/RT)(d\gamma/d \ln C) \quad (6)$$

where: **T** is absolute temperature, R is universal gas constant (R = 8.314 x 10^7 ergs mol^{-1} K^{-1}), and dγ/d InC is surface activity. The Γ_{max} values in Table 5 were used to calculate the average minimum area per adsorbed molecule at the aqueous–air interface at saturated condition (A_{min}) using the following relationship [**41]:**

$$A_{min.} = 10^{16}/(N_A.\ \Gamma_{max}) \quad (7)$$

where: N_A is "Avogadro's number = 6.023 x 10^{23} molecule/mole"

3. 5. Thermodynamic Parameters of Surface Tension

The ability for micellization processes depends on the thermodynamic parameter (standard free energy, $\Delta G_{mic.}$). Most information on the free energy of micellization has been obtained indirectly through the CMC **[42].** The $\Delta G_{mic.}$ may be calculated by choosing the following expression equation (8) :

$$\Delta G_{mic} = RT\,(1-\alpha)\ln CMC \quad (8)$$

where R is the universal gas constant (R =8.314 J/mol. K), T is the absolute temperature, α is the fraction of counter ions bound by micelle in case of ionic surfactants (α=0 for nonionic surfactants) and CMC is the critical micelle concentration in mol/L. Many investigations deal with the thermodynamics of surfactant adsorption at the interface **[43].** The thermodynamic parameters value of adsorption ΔG_{ads} were calculated via the following equation (9):

$$\Delta G_{ads} = \Delta G_{mic} - 0.6023\,\Pi_{CMC}\,A_{min} \quad (9)$$

The free energy of micellization in **Table 4** indicates that the micellization process is spontaneous ($\Delta G_{mic} < 0$). The data show also that, the negativity of ΔG_{mic} for surfactants increased as follows (III > II > I) and this may be due to the effect of hydrophobic moieties on the head group. This behavior indicates that increasing the oxyethylene chain length favors the micellization process. From the data obtained, it was found that all ΔG_{ads} values are negative and they are more negative than ΔG_{mic} values. This indicates that, the adsorption at the interface is associated with a decrease in the free energy of the system i. e. the adsorption process is more spontaneous. Also, this indicates that, the studied surfactants favor adsorption than micellization.

3. 6. Adsorption Isotherm

The adsorption of inhibitor molecules on metal surface is a substitute process, in which the water molecules adsorbed on the metal surface are replaced by inhibitor molecules. In order to get a better understanding for the adsorption mechanism, the Langmuir adsorption isotherm equation was employed [**44]:**

$$C_{inh}/\theta = 1/K_{ads.} + C_{inh} \quad (10)$$

Where ɵ is the surface coverage, which can be calculated from the Polarization measurements, C_{inh} is the molar concentration of the inhibitor and K_{ads} is the standard adsorption equilibrium constant for the adsorption/desorption process. The plots of C_{inh}/θ versus C_{inh} yielded a straight line with a slope near1 at 25 ^{0}C as shown in **Fig. 8**. From the intercepts of the straight lines on the C_{inh}/θ -axis, one can calculate K_{ads}. This isotherm clearly revealed that the adsorption of the synthesized surfactants on the X70 steel pipeline surface obeyed the Langmuir adsorption isotherm and the inhibitor molecules are adsorbed on X70 steel pipeline surface forming a film, which prevents the X70 steel pipeline from corrosion induced by the medium. The values of K_{ads} are given in **Table 5** and indicated that the synthesized inhibitors possess strong adsorption ability onto the X70 steel pipeline surface. The standard adsorption equilibrium constant (K_{ads}) are related to the standard free energy of adsorption, ΔG^0_{ads}, as given by Eq. (11) [**45]:**

$$\Delta G^0_{ads} = -RT\ln(55.5\,K_{ads}) \quad (11)$$

The calculated free energy of adsorption (ΔG^0_{ads}) is given in **Table 5**. The negative values of ΔG^0_{ads} indicated that the adsorption of the inhibitors on the metal surface is spontaneous. Generally, values of ΔG^0_{ads}around -20 kJ mol^{-1} or lower are consistent with the electrostatic interaction between charged molecules and the charged metal surface (physisorption) [**46]** ; those around -40 kJ mol^{-1} or higher involve charge sharing or transfer from organic molecules to the metal surface to form a coordinate type of metal bond (chemisorption) [**44].** It can be seen from **Table 5** that, calculated ΔG^0_{ads}values indicated that the adsorption mechanism of the prepared surfactants on carbon steel in the deep oil well formation water is (physical adsorption). The large values of $\Delta G^0_{ads}$and its negative sign are usually characteristic of strong interaction and a highly efficient adsorption.

3. 7. Scanning Electron Microscopy (SEM)

Fig. 9a shows SEM image of polished carbon steel surface. The micrograph shows a characteristic inclusion, which was probably an oxide inclusion [**47]. Fig. 9b** shows SEM of the surface of carbon steel specimen after immersion in formation water for three days in absence of inhibitor, while **Fig. 9c** shows SEM of the surface of another carbon steel specimen after immersion in formation water for the same time interval in the presence of 500 ppm of the inhibitor (III). The resulting scanning

electron micrographs reveal that, the surface was strongly damaged in the absence of the inhibitor, but in the presence of 500 ppm of the inhibitor (III), there is less damage in the surface. This confirms the observed high inhibition efficiency of the inhibitor (III) at this concentration.

3. 8. Energy Dispersive Analysis of X-rays (EDX)

The EDX spectrum in **Fig. 10a** shows the characteristic peaks of some of the elements constituting the polished carbon steel surface. The spectrum of the polished carbon steel surface after immersion in the formation water in the absence and presence of inhibitor (III) for three days is shown in **Figs. 10b** and **10c** respectively. The spectrum of **Fig. 10c** shows that the Fe peak is considerably decreased relative to the samples in **Figs. 10a** and **10b**. This decreasing of the Fe band is indicated that strongly adherent protective film of inhibitor (III) formed on the polished carbon steel surface, which leads to a high degree of inhibition efficiency [**48].** Therefore, the EDX and SEM examinations of the carbon steel surface support the results obtained from the chemical and electrochemical methods that the synthesized surfactant inhibitors are a good inhibitor for the carbon steel in the oil wells formation water.

3. 9. Quantum Chemical Calculations

The effectiveness of an inhibitor can be related to its spatial molecular structure, as well as with their molecular electronic structure [**49].** Also there are certain quantum chemical parameters that can be related to the interactions of metal-inhibitor. Among these, we can mention the energy of the HOMO, which is often associated with the capacity of a molecule to donate electrons. Therefore, an increase in the values of E_{HOMO} can facilitate the adsorption and therefore the inhibition efficiency, by indicating the disposition of the molecule to donate orbital electrons to an appropriate acceptor with empty molecular orbitals. In the same way, low values of the energy gap $\Delta E = E_{LUMO}-E_{HOMO}$ will render good inhibition efficiencies, because the energy needed to remove an electron from the last occupied orbital will be low [**50].** Similarly, low values of the dipole moment μ will favor the accumulation of inhibitor molecules on the metallic surface [**51].** Geometric structures and electronic properties of (I, II and III) used as corrosion inhibitors were calculated by ab initio method with 3-21G** basis set. The quantum chemical parameters such as the energy of the highest occupied molecular orbital (E_{HOMO}, eV), the energy of the lowest unoccupied molecular orbital (E_{LUMO}, eV), the energy gap ($\Delta E=E_{LUMO}-E_{HOMO}$, eV), the dipole moment (μ, Debye), logP (lipophilicity) and the number of transferred electrons (ΔN) were calculated and listed in **Table 6**, and the fully optimized minimum energy geometrical configuration of the inhibitors is shown in **Fig. 11**. The linear correlation between E_{HOMO} energy level and the corrosion inhibition efficiency of the inhibitors proved that, the higher the HOMO energy of the inhibitor (less negative values), the greater the trend of offering electrons to the unoccupied d orbital of the metal and the higher the corrosion inhibition efficiency for steel X70in deep oil wells formation water under CO_2 and H_2S environments. In addition, the lower the LUMO energy, the easier the acceptance of electrons from the metal surface. In other words, the inhibition efficiency increases if the compound can donate electrons from its HOMO to the LUMO of the metal, whereby chelation on the metal surface occurs. Also, as the energy gap (ΔE) decreases, the efficiency of the inhibitor is improved. The order of increasing the values of E_{HOMO} and decreasing the values of E_{LUMO} and the energy gap (ΔE) with increasing the inhibition efficiency of I, II and III. From **Fig. 11**, it is clear that, for I and II the geometric structure of these inhibitors is tri angle look like structure which make good I. E. It can be observed that for III (built on aromatic alkyl halide) the benzene ring, has larger electric density coming from the pz orbital of Π bond. Low values of the dipole moment will favor the accumulation of inhibitor molecules on the metallic surface thus increasing the inhibition effectiveness [**51].** The lowest value of dipole moment was obtained by I (3.45), II (8.052) and III (8.058). According to Lukovits's study **[52],** if the value of $\Delta N < 3.6$, the inhibition efficiency increased with increasing electron donating ability of inhibitor at the metal surface**.** The values of (ΔN) showed in Table 6 represent the number of electronic charges that will be exchanged between the surface and the adsorbed species.

4. Conclusion

The conclusion of this work can be stated in the following points:

1. Three surfactants based on N, N'- (azanediylbis (ethane-2, 1-diyl)) dioleamide which named (I, II, and III) were synthesized and purified. The chemical structure of these compounds was confirmed by 1H NMR and FT-IR, and their surface properties were determined.
2. The prepared surfactants were examined as corrosion inhibitors. From all measurements performed, the prepared surfactants are good inhibitors for the corrosion of carbon steel in formation water. High inhibition efficiencies are observed around their CMCs, and the inhibition efficiency increases with increasing of inhibitor concentrations up to 500 ppm. The order of inhibition efficiency decreased as follows III > II > I.
3. Aromatic alkyl halide is the optimum to get the quaternary ammonium salts and have good inhibition efficiency.
4. The potentiodynamic polarization curves indicated that the inhibitors inhibit both anodic metal dissolution and cathodic hydrogen evolution reactions and acted as mixed type inhibitors in the test solution.
5. The adsorption of the inhibitor molecules on the metal surface from the test solution obeys Langmuir's adsorption isotherm. The adsorption process is spontaneous and act as physical adsorption.

References

[1] G. Trabanelli, Corrosion 47 (1991) 410.
[2] M. A. Hegazy, M. Abdallah, H. Ahmed, Corrosion Science 52 (2010) 2897.
[3] A. Hernández-Espejel, M. A. Domínguez-Crespo, R. Cabrera-Sierra, C. Rodríguez-Meneses, E. M. Arce-Estrada, Corrosion Science 52 (2010) 2258.
[4] DemetOzkır, KadriyeKayakırılmaz, EmelBayol, A. Ali Gurten, FatmaKandemirli, Corrosion Science 56 (2012) 143.
[5] S. Safak, B. Duran, A. Yurt, G. Turkoglu, Corrosion Science 54 (2012) 251.
[6] A. M. Al-Sabagh, N. Gh. Kandile, N. M. Nasser, M. R. Mishrif, Amira E. El-Tabey, Egyptian Journal of Petroleum 22 (2013) 351.
[7] Ahmed A. Farag, M. R. Noor El-Din, Corrosion Science 64 (2012) 174.
[8] S. M. Shaban, A. Saied, S. M. Tawfik, A. Abd-Elaal, I. Aiad, Journal of Industrial and Engineering Chemistry 19 (2013) 2004.
[9] M. A. Migahed, M. M. Attya, S. M. Rashwan, M. Abd El-Raouf, A. M. Al-Sabagh, Egyptian Journal of Petroleum 22 (2013) 149.
[10] E. E. Ebenso, P. C. Okafor, U. J. Ekpe, Anti-Corrosion Method M 37 (2003) 381.
[11] G. Bereket, A. Pinarbasi, C. Ogretir, Anti-Corrosion Method M 51 (2004) 282.
[12] M. A. Migahed, A. M. Al-Sabagh, E. G. Zaki, H. A. Mostafa and A. S. Fouda. Elixir Corrosion & Dye 77 (2014) 28958.
[13] A. Popova, M. Christov, S. Raicheva, E. Sokolova, CorrosionScience 46 (2004) 1333.
[14] D. Zhang, Zh. An, Q. Pan, L. Gao, G. Zhou, Corrosion Science 48 (2006) 1437.
[15] M. A. Migahed, Progress in Organic Coatings54 (2005) 91.
[16] J. W. Graves, E. H. Sullivan, Material Protection 5 (1996) 33.
[17] N. Muthukumar, S. Maruthamuthu, N. Palaniswamy, Colloids andSurfaces B: Biointerfaces 53 (2006) 260.
[18] X. Jiang, Y. G. Zheng, W. Ke, Corrosion Science 47 (2005) 2636.
[19] F. G. Liua, M. Du, J. Zhanga, M. Qiua, Corrosion Science 51 (2009) 102.
[20] D. Hardie, E. A. Charles, A. H. Lopez, Corrosion Science 48 (2006) 4378.
[21] Y. F. Cheng, International Journal of Hydrogen Energy 32 (2007) 1269.
[22] B. Brown, S. R. Parakala, S. Nesic, NACE International Corrosion Conference and Expo, 2004.
[23] D. W. Shoesmith, P. Taylor, M. G. Bailey, D. G. Owen, Journal of ElectrochemicalSociety 127 (1980) 1007.
[24] I. B. Obot, S. A. Umoren, N. O. Obi-Egbedi, Journal of Material and Environmental Science2 (2011) 60.
[25] A. A. Farag, M. R. Noor El-Din. Corrosion Science 64 (2012) 174.
[26] M. Motamedi, A. R. Tehrani-Bagha, M. Mahdavian. Corrosion Science 70 (2013) 46.
[27] M. M. Osman, A. M. A. Omar, A. M. Sabagh, Material Chemistry and Physics 50 (1997) 271.
[28] A. M. Al-Sabagh, N. Gh. Kandil, O. Ramadan, N. M. Amer, R. Mansour, E. A. Khamis Egyptian Journal of Petroleum 20 (2011) 47.
[29] G. Bereket, E. Hur, C. Og˘retir, Journal of Molecular Structure578 (2002) 79.
[30] W. Yinqiu, P. R. Herrington, JAOCS 74 (1997) 1.
[31] Y. Ohshiro, M. Ochiai, and S. Komori, Journal of Electrochemical Society 64 (1961) 114.
[32] A. M. Al-Sabagh, M. A. Migahed and H. S. Awad, Corrosion Science 48 (2006) 813.
[33] R. G. Andrew, M. M. Michael, M. P. Rama, Journal of Dispersion Science and Technology 27 (2006) 731.
[34] M. A. Migahed, H. M. Mohamed, A. M. Al-Sabagh, Material Chemistry and Physics 80 (2003) 169.
[35] C. Cao, Corrosion Science 38 (1996) 2073.
[36] M. A. Hegazy, Ali M. Hasan, M. M. Emara, Mostafa F. Bakr, Ahmed H. Youssef, Corrosion Science 65 (2012) 67.
[37] K. F. Khaled, Applied Surface Science 252 (2006) 4120.
[38] M. A. Migahed, M. M. Attya, M. Abd El-raouf, E. Khamis, T. A. Ali and A. M. Al-Sabagh, International Journal of Electrochemical Science 10 (2015) 1343.
[39] R. Oda, I. Hucb, J. Sauveur, Chemical Communi-cations 56 (1997) 2105.
[40] N. A. Negm, Journal of Surfactants and Detergent 10 (2007) 87.
[41] S. M. Hamid and D. C. Sherrington, Journal of British Polymer 16 (1984) 39.
[42] M. J. Rosen, Surfactants and Interfacial Phenomena, John Wileyand Son Inc. , New York, 2004.
[43] A. M. Al-Sabagh, D. R. K. Harding, N. G. Kandile, A. M. Badawi, A. E. El-Tabey, Journal of Dispersion Science and Technology 30 (2009) 472.
[44] A. Doner, R. Solmaz, M. Ozcan, G. Kardas, Corrosion Science 53 (2011) 2902.
[45] G. E. Badr, Corrosion Science 51 (2009) 2529.
[46] B. G. Ateya, B. E. El-Anadouli, F. M. A. El-Nizamy, Corrosion Science24 (1984) 497.
[47] ASTM E 45-87, vol. 11, ASTM, Philadelphia, PA, (1980) 125.
[48] M. A. Amin, Journal of Applied Electrochemistry 36 (2006) 215.
[49] H. Ashassi-Sorkhabi, B. Shaabani, D. Seifzadeh, ElectrochemicaActa 50 (2005) 3446.
[50] N. Khalil, ElectrochimicaActa 48 (2003) 2635.
[51] P. Molymeux, C. T. Rhodes, J. Swarbrick, Trans. Faraday Soc. 61 (1965) 1043.
[52] I. Ahamad, R. Prasad, M. A. Quraishi, Corrosion Science 52 (2010) 933.

List of Tables

Table 1: Physical properties and chemical composition of deep oil well formation water used in this investigation.

Property	**Unit**	**Value**
Density	g/cm3	1.206
Salinity as NaCl	ppm	303567
Resistivity	Ω. m	0.017
PH		6.380000
Ionic species	**Value (ppm)**	
Sulfate	600	
Chloride	183980	
Sodium	43760	
Iron	683	
Strontium	94	
Calcium	57720	
Magnesium	12	
Barium	7	
Lead	372	
Potassium	10930	
Zinc	374	

Table 2: Data obtained from potentiodynamic polarization measurements of carbon steel X70 immersed in deep oil well formation water in the absence and presence of various concentrations of the inhibitors (I, II and III) at 298K

Inhibitor	**Conc. (ppm)**	**E_{corr} (mV)**	**I_{corr}, (μAcm^2)**	**b_c (mV)**	**b_a (mV)**	**R_P (KΩcm^2)**	**θ**	**η_P (%)**
blank	-	-602.2	223	-169.1	105.1	0.26	-	-
Inhibitor I	100	-645.5	94.6	-251.2	182.2	0.62	0.576	57.6
	200	-652.3	71.9	-179.2	166.6	0.52	0.63	63
	300	-668.3	68.3	-242	190.5	0.77	0.694	69.4
	400	-643.2	59.5	-148.5	152.8	0.52	0.733	73.3
	500	-665	49.2	-161.5	163.2	0.7	0.779	77.9
Inhibitor II	100	-656.3	91.4	-159.6	137.8	0.42	0.59	59
	200	-651.3	72.7	-194.8	200.4	0.59	0.652	65.2
	300	-663.8	66.4	-194.7	169.7	0.66	0.702	70.2
	400	-664.9	59.3	-244.4	155.2	0.9	0.734	73.4
	500	-719.5	48.2	-167.8	114.5	0.64	0.784	78.4
Inhibitor III	100	-657.7	90.7	-224.6	175.8	0.57	0.593	59.3
	200	-656.1	77.7	-160.6	173	0.51	0.674	67.4
	300	-663.2	64.7	-181.8	155	0.66	0.71	71
	400	-707.6	59.3	-161	139.8	0.61	0.734	73.4
	500	-678. 4	47	-138	127.4	0.6	0.789	78.9

Table 3: Data obtained from electrochemical impedance spectroscopy (EIS) measurements of carbon steel in the test solution in the absence and presence of various concentrations of the inhibitors (I, II and III) at 298K.

Inhibitor	Conc. (ppm)	Rs (Ω cm^2)	C_f x10^{-5} (μFcm^{-2})	n	R_f (Ω cm^2)	C_{dl} x10^{-4} (μFcm^{-2})	n	R_{ct} (Ω cm^2)	η_I (%)
blank	-	3.9	2.4	0.8	13.17	16.41	0.8	166.4	-
Inhibitor I	100	4.33	3.76	0.94	21.36	14.01	0.61	334.94	50.32
	200	4.98	4.72	0.91	22.60	13.69	0.57	367.12	54.67
	300	5.96	17.2	0.73	36.09	13.12	0.63	404.46	58.86
	400	6.42	20.8	0.83	41.75	12	0.82	444.08	62.53
	500	7.82	17.9	0.42	5.47	10.8	1.15	596.58	72.11
Inhibitor II	100	4.39	6.61	0.86	2.02	23	0.58	336.18	50.5
	200	4.58	4.19	0.92	18.05	21.76	0.55	367.20	54.68
	300	5.94	5.21	0.82	29.20	16.67	0.61	405.23	58.94
	400	5.77	1.24	1.18	4.19	14.6	0.37	458.06	63.67
	500	6.19	10.7	0.78	35.44	13	0.58	603.29	72.42
Inhibitor III	100	6.85	5.27	0.88	21.99	24.82	0.60	336.50	50.55
	200	4.58	3.36	0.89	17.19	17.44	0.48	367.78	54.76
	300	5.38	6.27	0.88	28.42	15.66	0.59	411.12	59.53
	400	4.63	2.31	1.09	6.67	13.55	0.48	473.12	64.83
	500	7.26	51.36	0.32	2.24	11.8	1.07	631.64	73.66

Table 4: Surface active properties of the investigated surfactants at 298K.

Inhibitors	CMCx10^{-4} (mol L^{-1})	γ_{CMC} (mNm^{-1})	π_{CMC} (mNm^{-1})	Γ_{Max} x10^{10} (mol cm^{-2})	A_{min} ($A^{0\,2}$)	$\Delta G_{mic.}$ (kJ mol^{-1})	$\Delta G_{ads.}$ (kJ mol^{-1})
I	2	39. 3	33	1. 70	97. 7	-21. 1	-23. 05
II	2. 1	37. 67	34. 63	1. 70	97. 7	-20. 98	-23. 02
III	1. 9	37	35. 3	1. 70	97. 9	-21. 23	-23. 31

Table 5: Adsorption parameter of three inhibitors on carbon steel in test solution at 298K.

Inhibitors	R^2	$K_{ads.}$ x10^4 (M^{-1})	$\Delta G_{ads.}$ (KJ mol^{-1})
I	0. 995	4. 07	-14. 9
II	0. 996	4. 69	-15. 0
III	0. 996	5. 38	-15. 2

Table 6: Calculated quantum chemical parameters of studied inhibitors.

Inhibitors	E_{HOMO} (eV)	E_{LUMO} (eV)	ΔE (eV)	μ (debye)	LogP	The number of transferred electrons, ΔN
I	-8. 00	0. 788	8. 788	3. 45	8. 34	0. 386
II	-9. 741	0. 217	9. 958	8. 052	10. 09	0. 224
III	-2. 238	0. 203	2. 441	8. 058	11. 46	0. 213

*The theoretical values of absolute electro negativity of iron (X_{Fe}), the absolute hardness of iron (η_{Fe}) and the electronic chemical potential of iron (μ_{Fe}) are 7, 0 and -7 eV/mol, respectively.

List of Figures

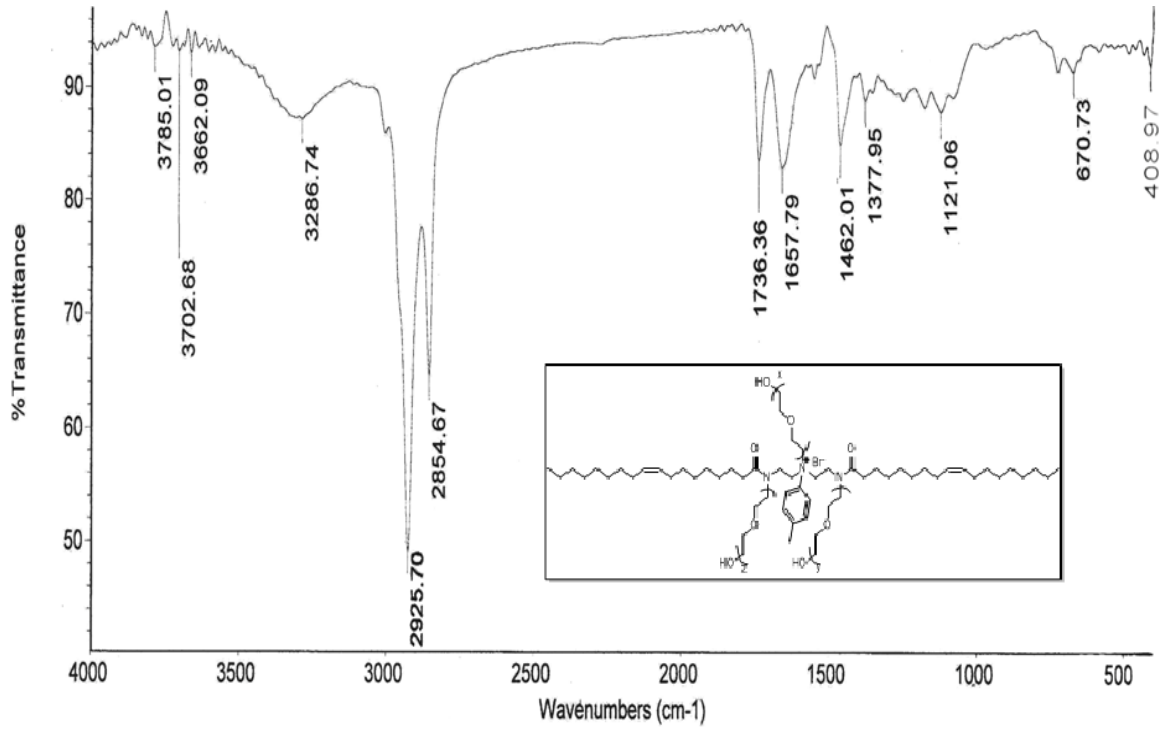

Figure 1: FTIR spectrum of inhibitor (III).

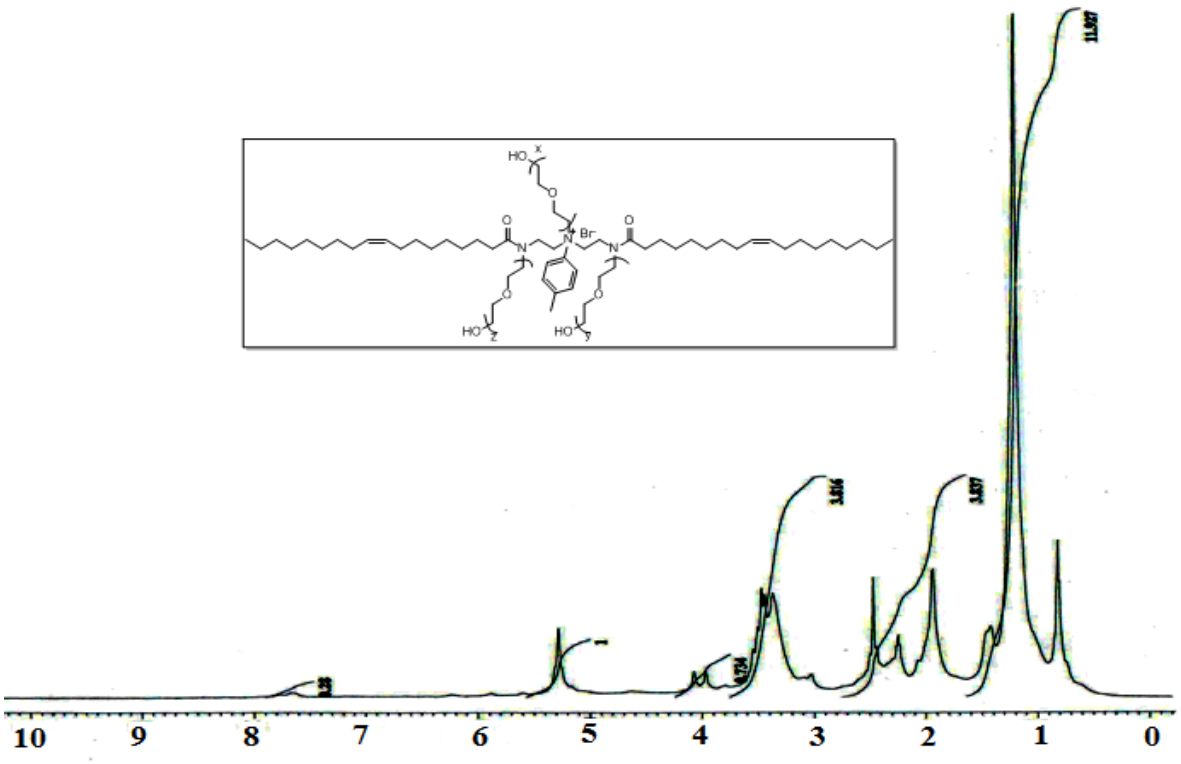

Figure 2: ^{1}H NMR spectrum of inhibitor (III).

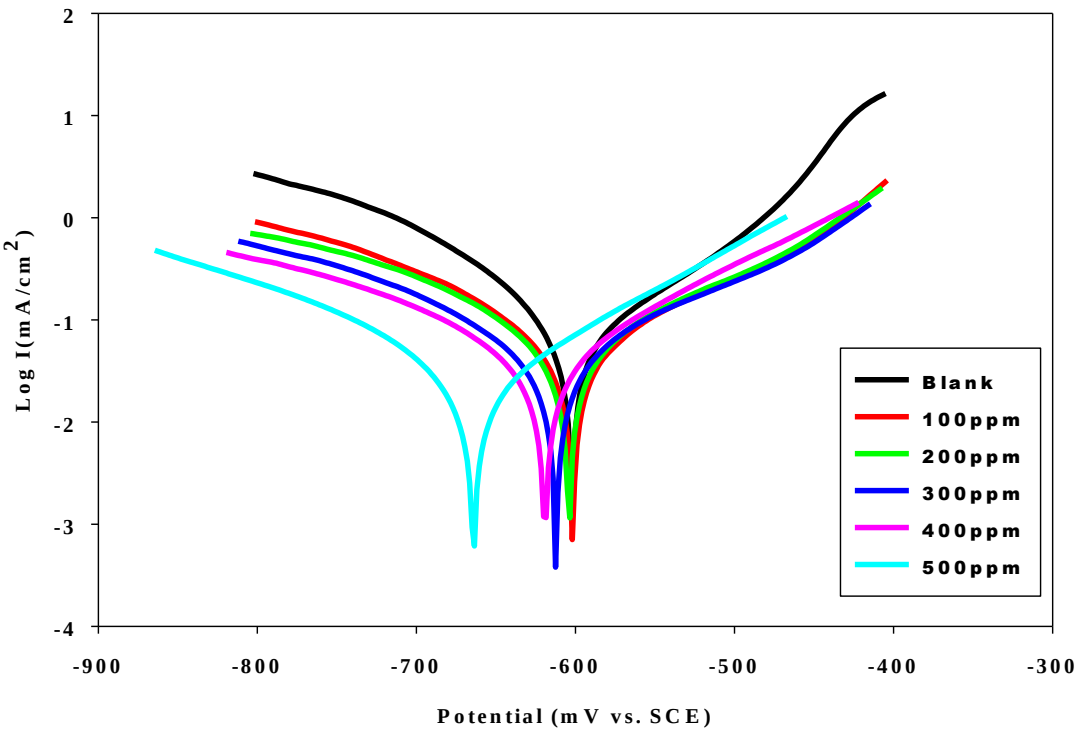

Figure 3: Potentiodynamic polarization curves (E – log I relationship) of carbon steel in the test solution in the absence and presence of different concentrations of inhibitor (III) at 298K.

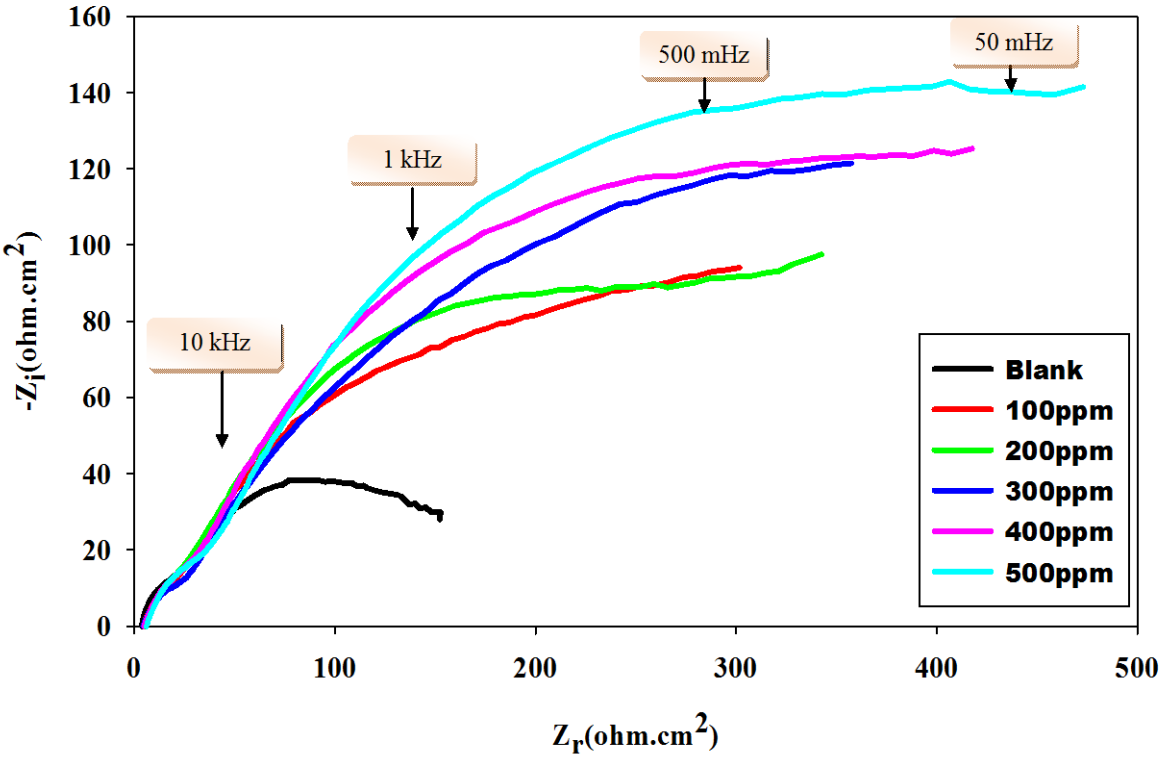

Figure 4: Nyquist plots for carbon steel in the test solution in the absence and presence of different concentrations of inhibitors (III).

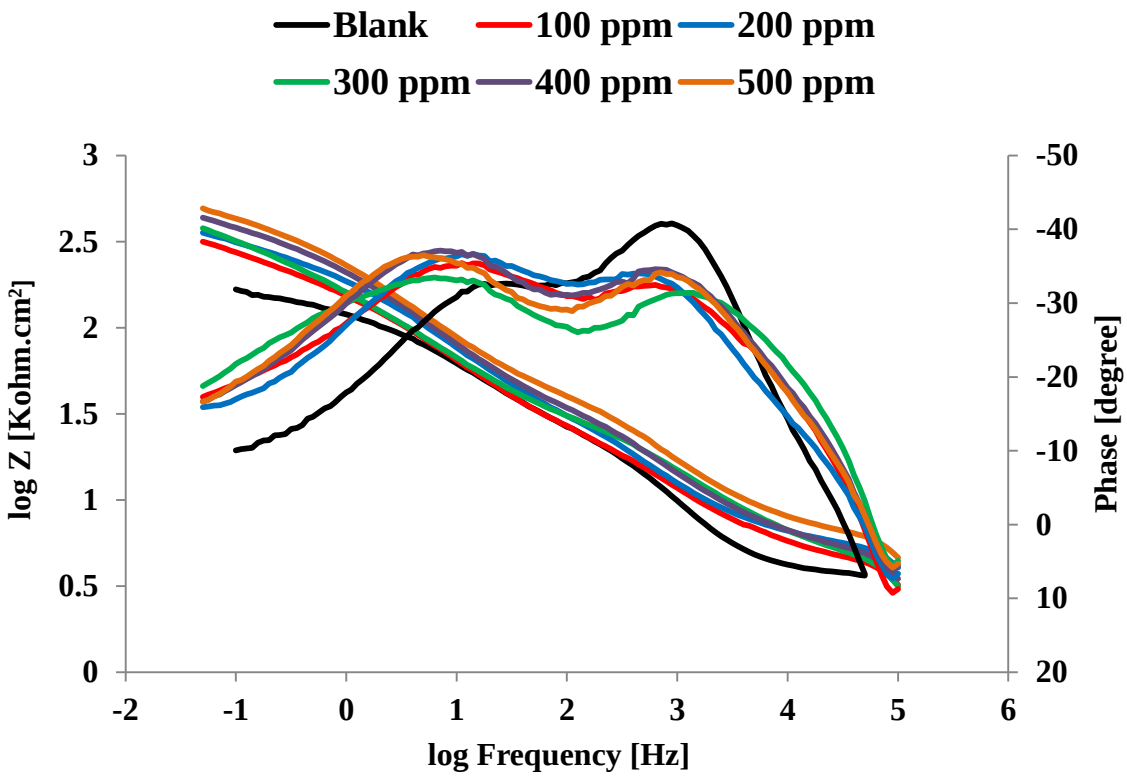

Figure 5: Bode plots for the carbon steel in the test solution in the absence and presence of various concentrations of inhibitor (III).

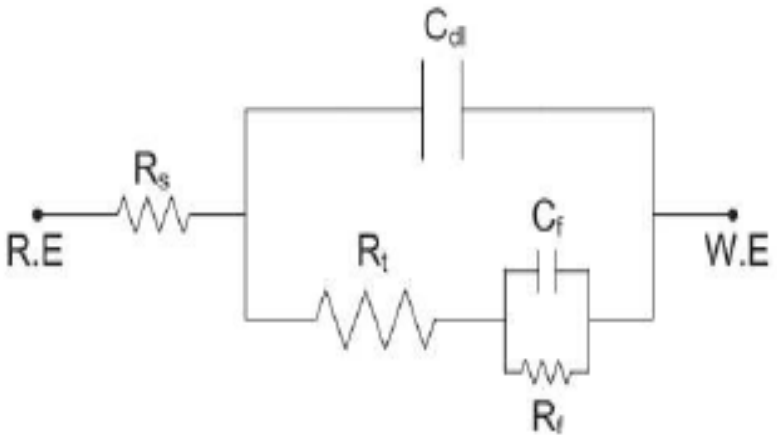

Figure 6: Equivalent circuit used to model impedance data of carbon steel in oil well formation water under CO_2 and H_2S environments.

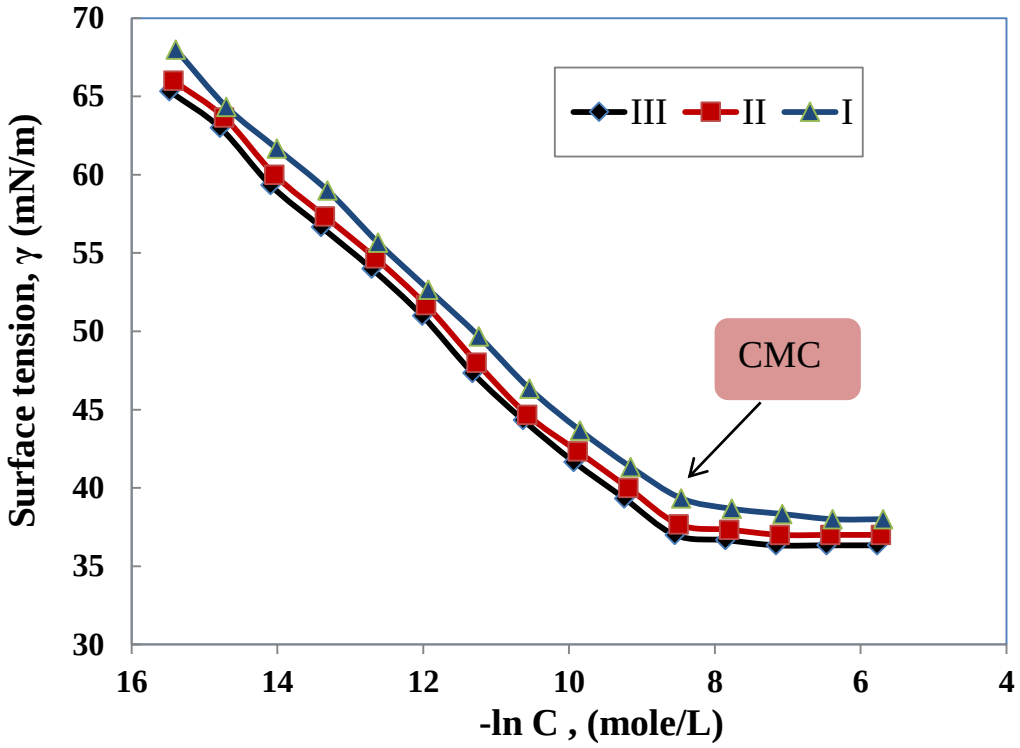

Figure 7: Surface tension (γ) vs. log C at different concentrations of the inhibitor (I, II and III) at 298K.

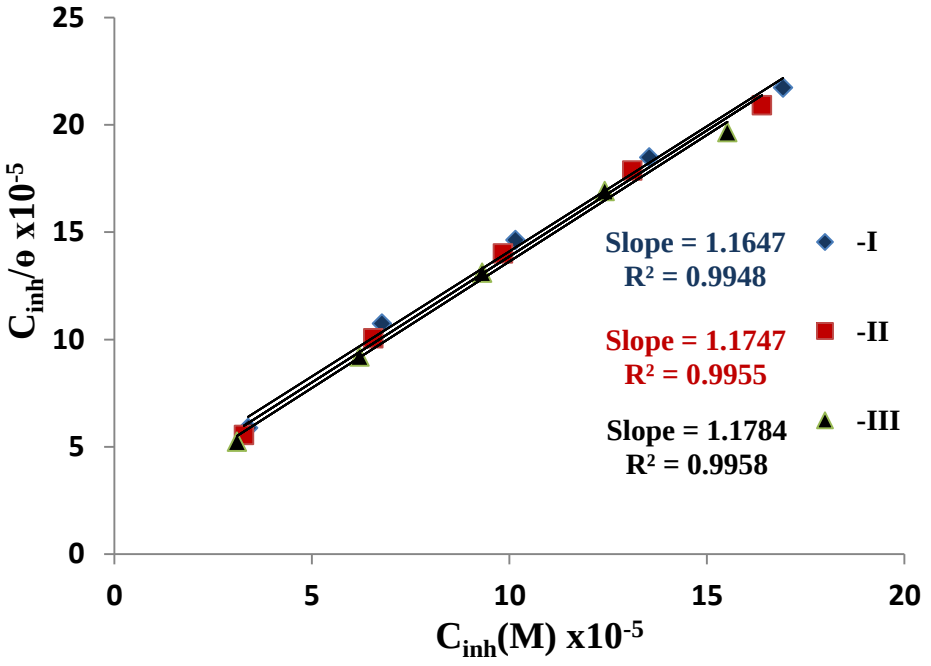

Figure 8: Langmuir isotherms for the adsorption of the prepared surfactants on carbon steel surface in test solution at 298K.

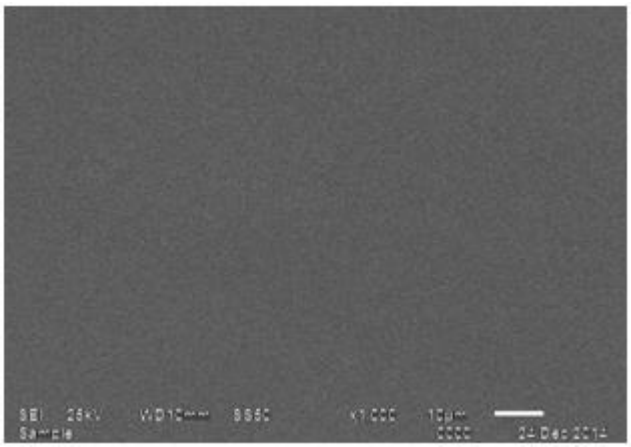

(a)

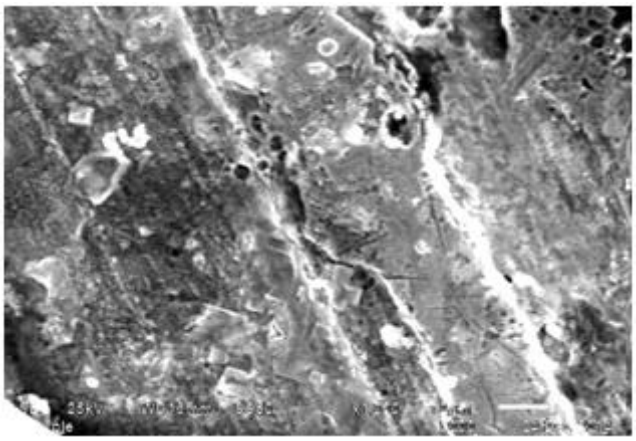

(b)

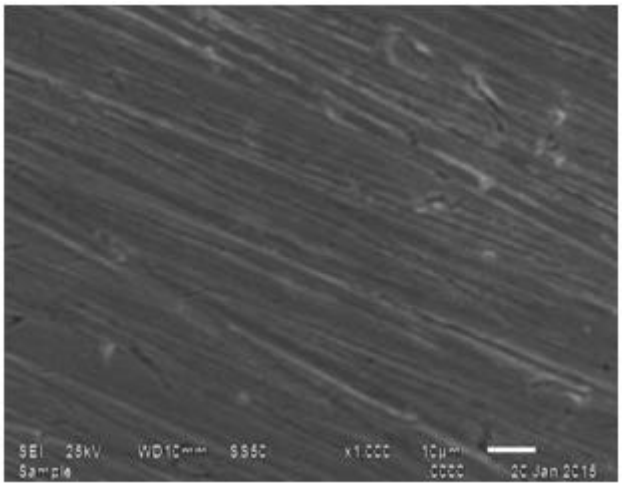

(c)

Figure 9: SEM of the carbon steel surface: (a) polished sample, (b) after immersion in the formation water and (c) after immersion in the formation water in the presence of 500 ppm of compound III.

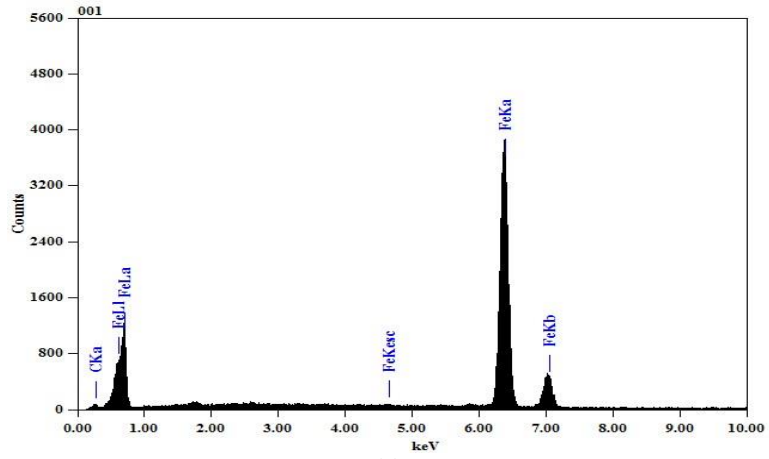

(a)

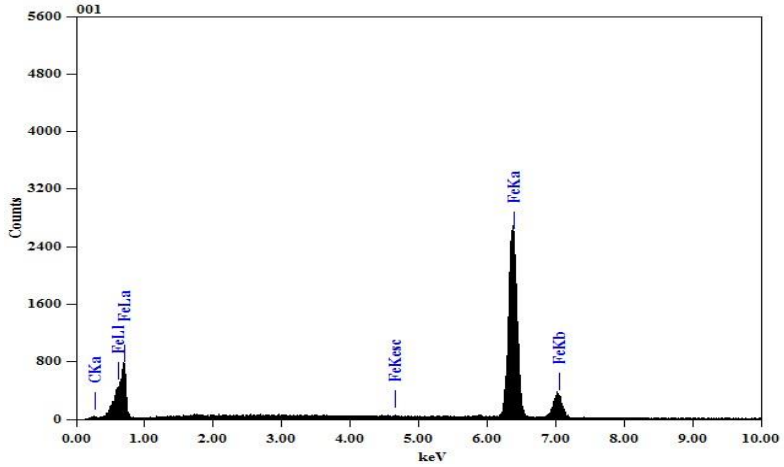

(b)

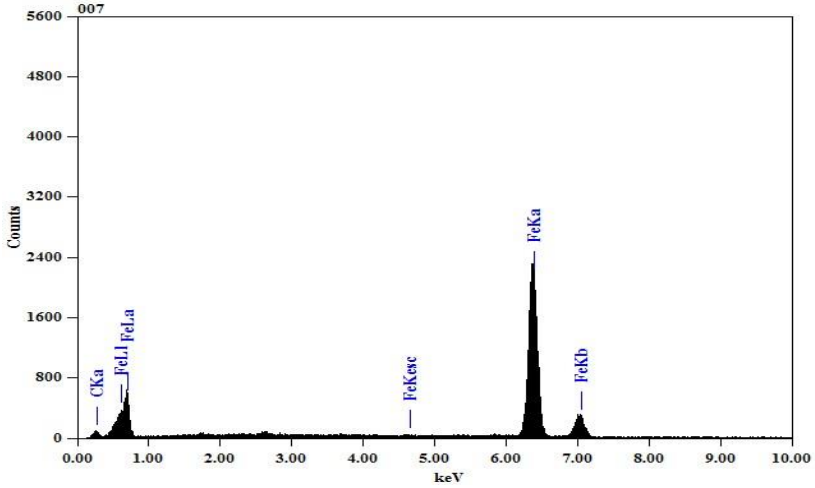

(c)

Figure 10: EDX of the carbon steel surface: (a) polished sample, (b) after immersion in the formation water and (c) after immersion in the formation water in the presence of 500 ppm of inhibitor (III).

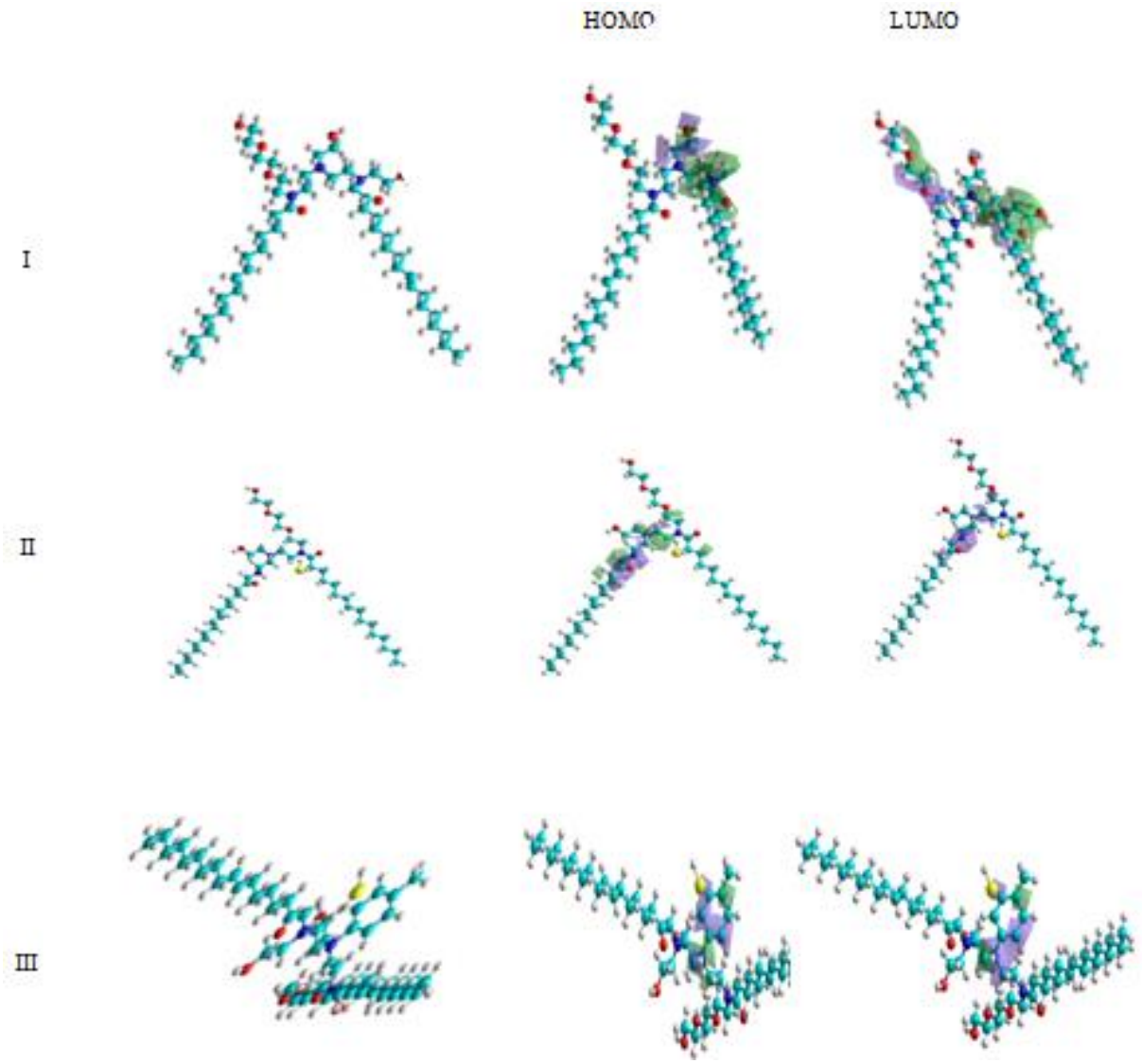

Figure 10: Molecular structure and HOMO–LUMO of compounds I, II and III.